Heliyon

Received:
8 October 2018
Revised:
14 February 2019
Accepted:
25 March 2019

Cite as:
Md. Moazzem Hossain. First-principles study on the structural, elastic, electronic and optical properties of $LiNbO_3$.
Heliyon 5 (2019) e01436.
doi: 10.1016/j.heliyon.2019.e01436

First-principles study on the structural, elastic, electronic and optical properties of $LiNbO_3$

Md. Moazzem Hossain [a,b,*]

[a] *Industrial Physics Division, BCSIR Laboratories Dhaka, BCSIR, Dhaka 1205, Bangladesh*

[b] *Department of Physics, University of Rajshahi, Rajshahi 6205, Bangladesh*

[*] Corresponding author.

E-mail address: mhsajib.ru@gmail.com (Md.M. Hossain).

Abstract

The structural, electronic, elastic, mechanical and optical properties of technologically important lithium niobate ($LiNbO_3$) have been investigated by using the first-principle calculations based on density functional theory (DFT) implemented in the CASTEP code. The lattice constants and unit cell volume were calculated from the optimized unit cell, which were in well agreement with the reported theoretical as well as experimental values. Bulk modulus B, Young's modulus Y, shear modulus G, Poisson's ratio σ, elastic anisotropy A and compressibility K were determined based on the computed values of independent elastic constants (C_{11}, C_{12}, C_{13}, C_{14}, C_{33}, C_{44} and C_{66}). Electronic band structure and density of states (DOS) demonstrated its semiconducting nature showing a band gap of 3.54 eV. Furthermore, several optical properties, such as absorption coefficient, reflectivity, refractive index, dielectric function, optical conductivity and electron energy loss function have been calculated.

Keyword: Condensed matter physics

https://doi.org/10.1016/j.heliyon.2019.e01436

1. Introduction

Perovskite compounds are of great interest to the researchers for several industrial and technological applications. Perovskite structure was first discovered by Gustav Rose in 1839. These materials exhibit unusual physical properties like high T_c superconductivity, ferromagnetism, ferroelectricity, spin dependent transport, high thermopower etc. The perovskite structures can be described by the common chemical formula ABO_3. In a cubic unit cell of this crystal structure, 'A' atom occupies corner positions (0, 0, 0) while 'B' atom is at body-center position (1/2, 1/2, 1/2) and oxygen atoms are at face centred positions (1/2, 1/2, 0).

In recent years, perovskite alkaline niobates ($ANbO_3$; A = Li, Na, K, Rb) are paying lots of attention due to their versatile properties for numerous applications, *e.g.* nonlinear optical response, piezoelectric, pyroelectric, photorefractive, and photocatalytic response as well as good mechanical and chemical stability.

Lithium niobate ($LiNbO_3$, LN) is ferroelectric material with layered structure [1]. It has attracted great interest as a future functional material due to their excellent ferroelectric, photorefractive, electro-optic, piezoelectric, nonlinear-optical, photocatalytic, and ion conductive properties [2, 3, 4, 5, 6]. Laser-induced optical damage also known as photorefraction was first observed in $LiNbO_3$ and $LiTiO_3$ crystals at the Bell Laboratories. For these excellent properties, I am interested to study several properties of this compound.

On the other hand, modern communication technology largely depends on fiber-optic systems. It includes laser as light sources, optical fiber, integrated optical components such as switches, modulators and optical detectors [7]. Different semiconducting materials are used to fabricate lasers and detectors. The integrated optical components are generally designed using single crystal materials such as $LiNbO_3$.

Substantial experimental and theoretical studies have been performed on $LiNbO_3$ [8, 9, 10, 11, 12, 13]. But, to the best of my knowledge, extensive theoretical study of elastic and mechanical properties is still lacking in literatures. Due to interesting unique physical properties of this compound, it is essential to know more details about the material. Density Functional Theory (DFT) is one of the most sophisticated tools in condensed matter physics to study different properties of a material. From this perspective, in the present work structural, elastic, electronic, thermodynamic and optical properties of lithium niobate ($LiNbO_3$) have been studied by using density functional theory (DFT).

2. Methodology

The simulation study was carried out using the pseudo-potential based plane-wave density functional theory (DFT) built in the CASTEP code [14, 15].

https://doi.org/10.1016/j.heliyon.2019.e01436

The core electrons were replaced by Vanderbilt type ultrasoft pseudopotentials [16] and plane-wave basis cut-off energy of 500 eV was used. Exchange correlation functional was taken into consideration using the local density approximation (LDA) with Ceperley−Alder and Perdew−Zunger (CA-PZ) functional [17, 18]. The potential of the constituent atoms was evaluated by assuming the neutral atomic configurations of Li $2s^1$, Nb $4d^4$ $5s^1$ and O $2s^2$ $2p^4$. The k-point mesh 9 × 9 × 3 of Monkhorst-Pack scheme was used for the calculations [19, 20]. The equlibrium structures were obtained by using Broyden-Fletcher-Goldfarb-Shenno (BFGS) methods [21]. The total energy was fixed to a value of 1.0×10^{-5} eV/atom; maximum force of 0.02 eV/Å; maximum stress of 0.04 GPa; maximum displacement of 0.001 Å and self consistent field of 1.0×10^{-6} Å.

Single crystal elastic constants have been calculated using stress-strain condition. The mechanical stability criteria also known as Born criteria for trigonal crystal system are as follows: [22, 23, 24]

$$C_{11} - C_{12} > 0;\ (C_{11} + C_{12})C_{33} - 2C_{13}^2 > 0;$$

$$(C_{11} - C_{12})C_{44} - 2C_{14}^2 > 0 \tag{1}$$

The bulk modulus B and shear modulus G are defined as,

$$B = \frac{1}{2}(B_{\mathrm{V}} + B_{\mathrm{R}}) \text{ and } G = \frac{1}{2}(G_{\mathrm{V}} + G_{\mathrm{R}}) \tag{2}$$

The well-known Young's modulus Y and Poisson's ratio σ are calculated using the following relations:

$$E = \frac{9BG}{3B + G} \tag{3}$$

$$\sigma = \frac{3B - 2G}{6B + 2G} \tag{4}$$

Further, elastic anisotropies such as compression anisotropy (A_{comp}) and shear anisotropy (A_{shear}) can be defined as [25].

$$A_{comp} = \frac{B_V - B_R}{B_V + B_R} \times 100\% \tag{5}$$

$$A_{shear} = \frac{G_V - G_R}{G_V + G_R} \times 100\% \tag{6}$$

https://doi.org/10.1016/j.heliyon.2019.e01436

3. Results and discussion

3.1. Structural properties

The $LiNbO_3$ crystallizes in trigonal structure of hexagonal symmetry with ten atoms per unit cell. At room temperature it exists in ferroelectric phase with space group R3c (no. 161) and change into para-electric phase ($R\overline{3}c$) above 1480K temperature [26]. The Wyckoff positions of atoms for this compound are Li (0, 0, 0.2829); Nb (0, 0, 0) and O (0.0492, 0.3446, 0.0647) [27]. The schematic crystal structure of $LiNbO_3$ is shown below in Fig. 1. The optimized lattice constants and related cell volume are presented in Table 1.

3.2. Elastic and mechanical properties

Elastic constants are fundamental properties of solid materials. The propagation of elastic wave through a medium depends on elastic constants of that material. Elastic properties are also linked to thermodynamic properties like specific heat, thermal expansion coefficient, Debye temperature and melting point. The elastic stiffness constants describe the response of a material to external applied forces. Elastic constants are used to describe the mechanical properties of solids. Bulk modulus, Young's modulus, shear modulus and Poisson's ratio are calculated from single crystal elastic constants which determine the hardness and strength of the material. Elastic constants are also related to the melting temperature of a solid.

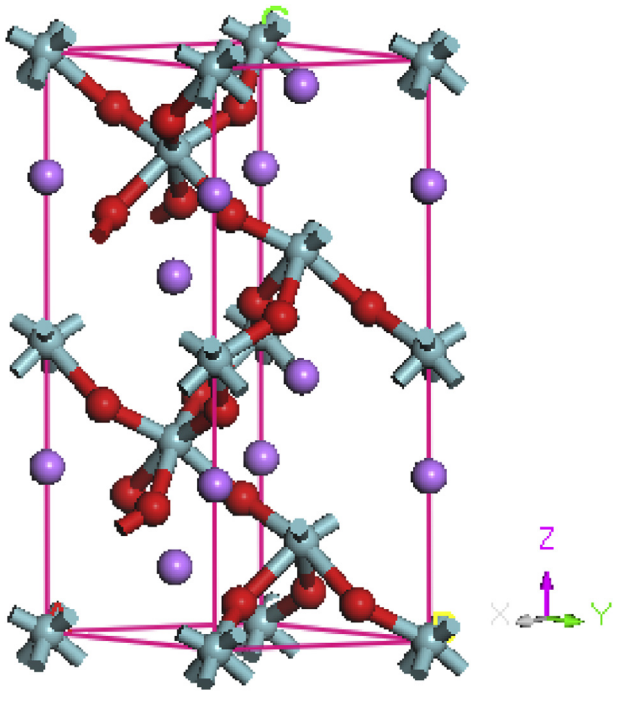

Fig. 1. Crystal structure of $LiNbO_3$.

https://doi.org/10.1016/j.heliyon.2019.e01436

Table 1. The optimized lattice constants and unit cell volume of $LiNbO_3$.

a (Å)	*b* (Å)	*c* (Å)	*c/a*	*V* (Å^3)	References
5.057	5.057	13.942	2.76	308.58	This work
5.221	5.221	14.094	2.70	332.71	[28]$^{theor.}$
5.159	5.159	13.869	2.69	320.18	[29]$^{theor.}$
5.147	5.147	13.849	2.69	317.73	[30]$^{expt.}$

For a trigonal crystal system 21 independent elastic stiffness constants reduce to seven components, C_{11}, C_{33}, C_{44}, C_{66}, C_{12}, C_{13} and C_{14} due to the presence of symmetry between stress and strain tensors.

The six independent elastic constants for $LiNbO_3$ obtained using stress-strain condition from CASTEP calculation are listed in Table 2, which satisfy the Born criteria mentioned in Eq. (1). Among the three diagonal components, C_{44} is smaller than C_{11} and C_{33}, which means that the material is easier to compress along the direction C_{44} than that of along the other two directions. On the other hand C_{33} shows the highest value. The calculated values were compared with reported experimental results and showed good agreement.

To study the polycrystalline behavior of a material from single crystal elastic constants, the well-established Voigt and the Reuss approximations are generally used [33, 34, 35].

The results are shown in Table 3. Bulk modulus is a very important mechanical property of solid materials. It indicates the ability of a material to resist compression under applied force and also represents the nature of chemical bonding in solids. The shear modulus measures resistance to shape change in materials. The higher the shear modulus, the more rigid the material is. Pugh established a ratio of *B/G*, which describes the ductile or brittle characteristics of materials which is very important for engineering applications. The cutoff value is 1.75. When $B/G > 1.75$, the material behaves in a ductile manner, otherwise, it exhibits brittle properties [36]. From Table 3, *B/G* ratio is 1.97 which indicates that $LiNbO_3$ should behave in ductile nature.

Table 2. Calculated single crystal elastic constants (C_{ij}) at external pressure $P = 0$.

C_{11}	C_{12}	C_{13}	C_{14}	C_{33}	C_{44}	C_{66}	References
205.69	69.28	72.15	12.38	238.34	65.81	70.03	This work
200	56	75	8	240	60	72	[31]$^{expt.}$
208.77	73.28	75.99	15.68	236.23	49.80	67.74	[29]$^{theor.}$
198.9	54.7	67.3	7.8	233.7	70.4	72.1	[32]$^{theor.}$

https://doi.org/10.1016/j.heliyon.2019.e01436

Table 3. Calculated bulk modulus B (GPa), Young's modulus E (GPa), shear modulus G (GPa), Poisson's ratio σ, and B/G ratio.

B	E	G	σ	B/G
272.80	355.95	138.77	0.28	1.97

Calculated A_{comp} and A_{shear} were found to be 8.37% and 21.90% respectively, which indicate that shear anisotropy is more serious than compression.

3.3. Electronic properties

3.3.1. Band structure and electronic density of states (DOS)

The spectrum of energy eigen values of a periodic system is band structure. The calculation of the band structure helps one to understand the shape of the Fermi surface. The electronic and optical properties of a compound can be understood by identifying the dominant bands near the Fermi level, their energy etc. The band gap is one of the most useful aspects of the band structure, as it influences strongly the electrical and optical properties of the material. The electronic band structure of $LiNbO_3$ is shown in Fig. 2(a).

The energy band structure of $LiNbO_3$ was computed at equilibrium volume ($P = 0$, which means equilibrium volume at zero pressure) by using the first principles DFT approach with local density approximation (LDA). The energy bands of $LiNbO_3$ are along the high symmetry direction, (F-Γ-Z) of the Brillouin zone in the energy range from -6 to $+10$ eV. The Fermi level is chosen at zero value of energy. The valence band maximum and conduction band minimum occur at the same point Γ, making it a direct band gap material. The calculated band gap of $LiNbO_3$ is $E_g = 3.54$ eV which is very close to the experimental value [37, 38, 39].

The electronic density of states (DOS) of a material is defined as the number of electronic energy states per unit energy at each energy level that are available to be occupied by the electrons.

The total and partial electronic density of states of $LiNbO_3$ at zero pressure ($P = 0$) are shown in Fig. 2(b) to describe the electronic structure. Here, the vertical line indicates the Fermi level, E_F. The partial contributions of s, p and d orbital of Li, Nb and O are displayed in the figure. The figure shows that the valence band and conduction band are composed of Li 2s, Nb 4d and O 2p. The lowest energy bands from -10 to $+10$ eV are mainly derived from the Nb 4d O and 2p states with little contribution of Li 2s state.

The atomic bonding nature has been represented clearly in partial DOS. The highest contribution of partial DOS comes from O 2p indicating a value of 5.15 states/eV

https://doi.org/10.1016/j.heliyon.2019.e01436

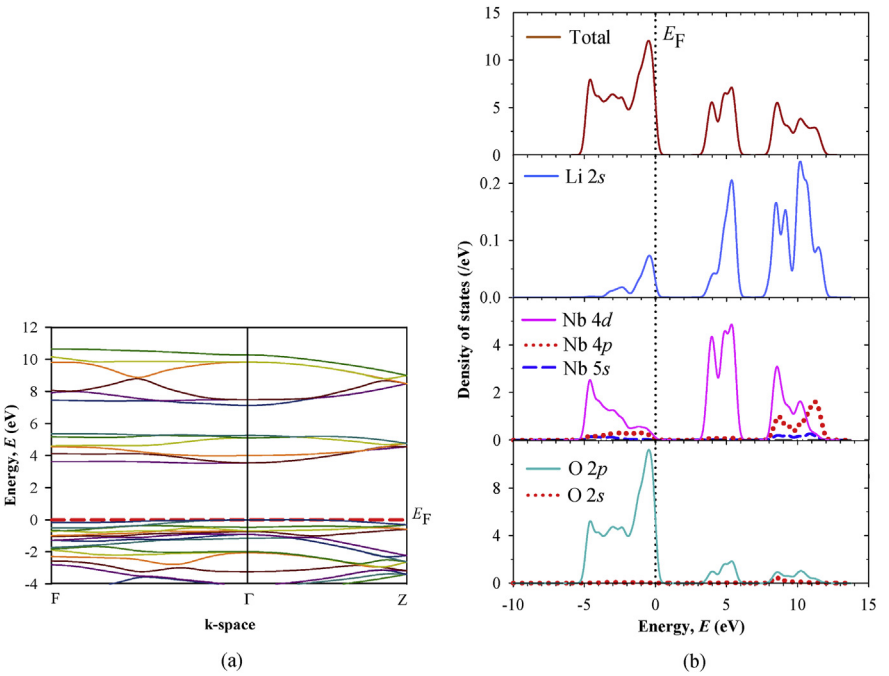

Fig. 2. (a) Electronic band structure and (b) total and partial density of states (DOS) of $LiNbO_3$.

which is the common characteristics of oxide semiconductors. Density of states for $LiNbO_3$ are listed in Table 4.

3.3.2. Mulliken populations: atomic and bond overlap

Mulliken populations are used to study the bonding nature of atoms in a crystal. Positive value of population represents bonding state whereas negative value indicate antibonding. Mulliken atomic and bond populations of $LiNbO_3$ are listed in Table 5.

3.4. Optical properties

The investigation of optical properties of a material is very important for various applications like absorbers, optical coatings, reflectors, and different optoelectronic devices. To understand the material response to incident electromagnetic radiation optical properties are essential. The response to electromagnetic radiation is

Table 4. Total and partial density of states of $LiNbO_3$.

Partial Density of States (States/eV)						**Total DOS (States/eV)**
Li	**Nb**			**O**		
2*s*	4*p*	4*d*	5*s*	2*s*	2*p*	5.30
0.03	0.22	0.23	0.08	0.02	5.15	

https://doi.org/10.1016/j.heliyon.2019.e01436

Table 5. Mulliken populations.

Atom	Mulliken populations of $LiNbO_3$				
	s	*p*	*d*	*f*	Total
Li	1.68	0.00	0.00	0.00	1.68
O	1.84	4.91	0.00	0.00	6.75
Nb	2.32	6.72	3.03	0.00	12.07

measured by the various optical parameters with respect to photon energy, such as real and imaginary parts of dielectric constant $\varepsilon_1(\omega)$ and $\varepsilon_2(\omega)$, respectively, complex refractive index having real part $n(\omega)$, extinction coefficient $k(\omega)$, real and imaginary parts of optical conductivity $\sigma_1(\omega)$ and $\sigma_2(\omega)$, respectively, reflectivity $R(\omega)$, absorption coefficient $\alpha(\omega)$ and loss function. Several optical parameters of $LiNbO_3$ were calculated for energies of incident radiation up to 20 eV as shown in Fig. 3 along electric field polarization vector [100].

The complex dielectric function $\varepsilon(\omega) = \varepsilon_1(\omega) + i\varepsilon_2(\omega)$ completely describes the optical properties of a medium for different photon energies. The peak value of real part of the dielectric constant is related the electron excitation. The real part can be derived from the imaginary part $\varepsilon_2(\omega)$ by the Kramers-Kronig relation. By using the momentum matrix elements between the occupied and the unoccupied states imaginary part of dielectric constant $\varepsilon_2(\omega)$ can be calculated.

The real and the imaginary parts of complex dielectric constant for $LiNbO_3$ are shown in Fig. 3(a). $LiNbO_3$ exhibits semiconducting characteristics in the energy ranges for which $\varepsilon_1(\omega) > 0$. For the real part $\varepsilon_1(\omega)$ of the dielectric function, the highest peak for $LiNbO_3$ appears at around 3.78 eV. On the other hand the imaginary

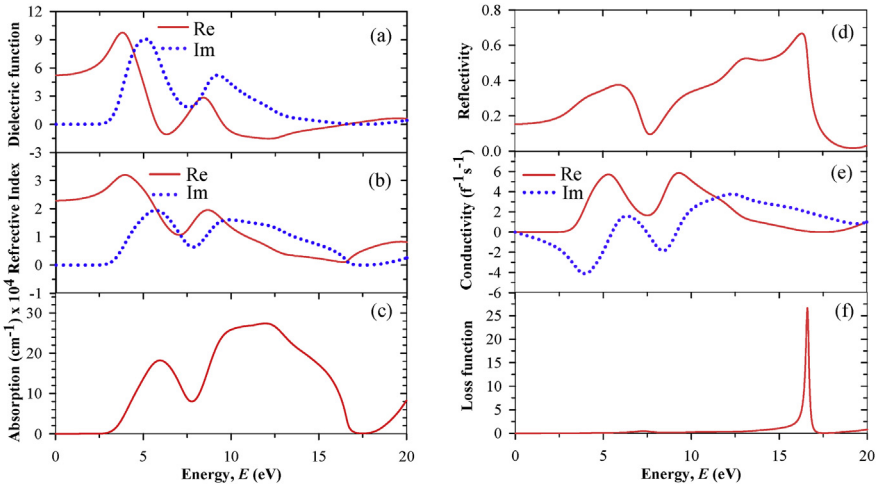

Fig. 3. (a) Dielectric constant, (b) refractive index, (c) absorption coefficient, (d) reflectivity, (e) optical conductivity and (f) loss function of $LiNbO_3$ as a function of energy.

https://doi.org/10.1016/j.heliyon.2019.e01436

part $\varepsilon_2(\omega)$ is indicating its first peak at 5.12 eV with the first edge at 3.25 eV, which is associated to the fundamental band gap, E_g.

The complex refractive index as a function of energy in eV is shown in Fig. 3(b). The static refractive index $n(0)$ was found to be 2.30 which agree with other reported theoretical and experimental values [40, 41]. The real part of refractive index, n is not zero at any energy whereas imaginary part of refractive index also known as extinction coefficient, k is zero at certain energy. The real part of the refractive index is a measure of phase velocity of the electromagnetic wave in a medium, while the imaginary part determines the attenuation of electromagnetic wave traveling through a material. The complex dielectric function is related to the real and imaginary parts of the refractive index by the expression, $\varepsilon(\omega) = n^2(\omega) - k^2(\omega)$ [42]. Therefore, at high photon energies both real and imaginary parts of the complex refractive index decrease since the imaginary part of the dielectric constant tends to zero as displayed in Fig. 3(a).

The absorption coefficient determines the solar energy conversion efficiency and it indicates how far light of a specific energy (frequency) can penetrate into the material before absorption. A strong absorption peak was found at 6.02 eV as shown in Fig. 3(c). Absorption stars at around 3.40 eV which is the band gap of the material. This confirms that, the material is partially transparent in visible region.

The reflectivity spectrum as a function of photon energy is shown in Fig. 3(d). For $LiNbO_3$ maximum reflectivity occurs at around 16.34 eV. This means that these materials may be used as promising materials for coatings in visible range.

The real ($\sigma_1(\omega)$) and imaginary ($\sigma_2(\omega)$) parts of optical conductivity are shown in Fig. 3(e). The first edge is found at 3.40 eV which corresponds to the fundamental band gap. The maximum conductivity was found to be 5.35 $f^{-1}s^{-1}$.

Fig. 3(f) shows the energy dependent loss function. The energy loss function, $L(w)$ of a material determines loss of energy of fast electron when it traverse through the medium. The maximum energy loss is 25.16 which occurs at around 16.65 eV indicating the bulk screened plasma frequency, ω_p of the compound which was compared with available reported data and showed good agreement [43]. The loss spectrum is highly isotropic with respect to the polarization of the incident electromagnetic wave.

4. Conclusions

In the present work, structural, electronic, elastic and optical properties of $LiNbO_3$ have been studied by means of first principles calculations. The elastic properties have been investigated, which followed the Born stability criteria. Several mechanical properties, like as Bulk modulus, Young's modulus, shear

https://doi.org/10.1016/j.heliyon.2019.e01436

modulus, and anisotropy factor were computed by using the values of C_{ij}. Young's modulus is very important parameter for industrial and technological applications of a material, which measures the stiffness of solids. The material showed high value of Young's modulus of 355 GPa. Both Pugh's ratio and Poisson's ratio confirmed the ductile nature of the compound. The electronic structure confirmed that the compound is a wide band gap semiconductor of 3.54 eV. The calculated value of real part of dielectric constant for $LiNbO_3$ is 3.75 at low energy and increased gradually to reach its highest value of 9.80 at 3.78 eV. The imaginary part of dielectric constant showed its first edge at around 3.25 eV, which is consistent with the fundamental band gap. The maximum value of static refractive index was found to be 3.47 at 4.35 eV. Based on the predicted properties, it may be concluded that the study will play an important role to develop modern technologies.

Declarations

Author contribution statement

Md. Moazzem Hossain: Conceived and designed the analysis; Analyzed and interpreted the data; Wrote the paper.

Funding statement

This research did not receive any specific grant from funding agencies in the public, commercial, or not-for-profit sectors.

Competing interest statement

The authors declare no conflict of interest.

Additional information

No additional information is available for this paper.

References

[1] A.A. Belik, T. Furubayashi, H. Yusa, E. Takayama-Muromachi, Perovskite, $LiNbO_3$, corundum, and hexagonal polymorphs of $(In_{1-x}M_x)MO_3$, J. Am. Chem. Soc. 133 (24) (2011) 9405−9412.

[2] D. Xue, X. He, Dopant occupancy and structural stability of doped lithium niobate crystals, Phys. Rev. B 73 (6) (2006), 064113.

https://doi.org/10.1016/j.heliyon.2019.e01436

[3] R.K. Choubey, P. Sen, P.K. Sen, R. Bhatt, S. Kar, V. Shukla, K.S. Bartwal, Optical properties of MgO doped $LiNbO_3$ single crystals, Opt. Mater. 28 (5) (2006) 467−472.

[4] O. Beyer, I. Breunig, F. Kalkum, K. Buse, Photorefractive effect in iron-doped lithium niobate crystals induced by femtosecond pulses of 1.5μm wavelength, Appl. Phys. Lett. 88 (5) (2006), 051120.

[5] G. Yang, Y. Kong, W. Hou, Q. Yan, Heating behavior and crystal growth mechanism in microwave field, J. Phys. Chem. 109 (4) (2005) 1371−1379.

[6] B. Yu, B. Cao, H. Cao, X. Zhang, D. Chen, J. Qu, H. Niu, Synthesis and nonlinear optical properties of single-crystalline KNb_3O_8 nanowires, Nanotechnology 24 (8) (2013), 085704.

[7] S. Oikawa, T. Kawanishi, K. Higuma, Y. Matsuo, M. Izutsu, Double-stub structure for resonant-type optical modulators Using 20- μm -thick electrode, IEEE Photon Tech. Lett. 15 (2) (2003) 221−223.

[8] R.F. Ali, B.D. Gates, Synthesis of lithium niobate nanocrystals with size focusing through an Ostwald Ripening process, Chem. Mater. 30 (6) (2018) 2028−2035.

[9] R. Hernandez-Molina, J.A. Hernandez-Marquez, J.L. Enriquez-Carrejo, J.R. Farias-Mancilla, P.G. Mani-Gonzalez, E.V. Santiago, M.C. Rodriguez, A. Vargas-Ortiz, J.M. Yanez-Limon, Synthesis by wet chemistry and characterization of $LiNbO_3$ nanoparticles, Superficies y Vacio 28 (4) (2015) 115−118.

[10] F. Dutto, C. Raillon, K. Schenk, A. Radenovic, Nonlinear optical response in single alkaline niobate nanowires, Nano Lett. 11 (6) (2011) 2517−2521.

[11] R.M. Araujo, M.E.G. Valerio, R.A. Jackson, Computer modeling of Hafnium doping in lithium niobate, Crystals 8 (3) (2018) 123.

[12] S. Mamoun, A.E. Merad, L. Guilbert, Energy band gap and optical properties of lithium niobate from ab initio calculations, Comp. Mater. Sci. 79 (2013) 125−131.

[13] S.M. Young, F. Zheng, M. Rappe, First-principles materials design of high-performing bulk photovoltaics with the $LiNbO_3$ structure, Phys. Rev. Appl. 4 (5) (2015), 054004.

[14] A.D. Becke, Perspective: fifty years of density-functional theory in chemical physics, J. Chem. Phys. 140 (18) (2014) 18A301.

https://doi.org/10.1016/j.heliyon.2019.e01436

[15] M.D. Segall, P.J.D. Lindan, M.J. Probert, C.J. Pickard, P.J. Hasnip, S.J. Clark, M.C. Payne, First-principles simulation: ideas, illustrations and the CASTEP code, J. Phys. Condens. Matter 14 (11) (2002) 2717–2744.

[16] D. Vanderbilt, Soft self-consistent pseudopotentials in a generalized eigenvalue formalism, Phys. Rev. B 41 (11) (1990) 7892(R).

[17] D.M. Ceperley, B.J. Alder, Ground state of the electron gas by a stochastic method, Phys. Rev. Lett. 45 (7) (1980) 566.

[18] J.P. Perdew, A. Zunger, Self-interaction correction to density-functional approximations for many-electron systems, Phys. Rev. B 23 (10) (1981) 5048.

[19] H.J. Monkhorst, J.D. Pack, Special points for Brillouin-zone integrations, Phys. Rev. B 13 (12) (1976) 5188.

[20] J.D. Pack, H.J. Monkhorst, Special points for Brillouin-zone integrations-a reply, Phys. Rev. B 16 (4) (1977) 1748.

[21] T.H. Fischer, J. Almlof, General methods for geometry and wave function optimization, J. Phys. Chem. 96 (24) (1992) 9768–9774.

[22] M. Born, K. Huang, Dynamics Theory of Crystal Lattices, Oxford University Press, 1954.

[23] G.V. Sin'ko, N.A. Smirnov, Relative stability and elastic properties of hcp, bcc, and fcc beryllium under pressure, Phys. Rev. B 71 (21) (2005) 214108.

[24] G.V. Sin'ko, N.A. Smirnov, Ab initio calculations of elastic constants and thermodynamic properties of bcc, fcc, and hcp Al crystals under pressure, J. Phys. Condens. Matter 14 (29) (2002) 6989.

[25] K.B. Panda, K.S.R. Chandran, Determination of elastic constants of titanium diboride (TiB_2) from first principles using FLAPW implementation of the density functional theory, Comp. Mater. Sci. 35 (2) (2006) 134–150.

[26] K. Toyoura, M. Ohta, A. Nakamura, K. Matsunaga, First-principle study on phase transition and ferroelectricity in lithium niobate and tantalite, J. Appl. Phys. 118 (6) (2015), 064103.

[27] S.C. Abrahams, E. Buehler, W.C. Hamilton, S.J. Lapaca, Ferroelectric lithium tantalate—III. Temperature dependence of the structure in the ferroelectric phase and the para-electric structure at 940°K, J. Phys. Chem. Solids 34 (3) (1973) 521–532.

[28] X. Liu, W. Qu, Y. He, H. Zhou, A first-principle study on the electronic properties of substitutionally Cu (I, II)-doped $LiNbO_3$, J. Adv. Dielectr. 8 (1) (2018) 1820002.

https://doi.org/10.1016/j.heliyon.2019.e01436

[29] S.K. Tripathy, G. Sahu, Ground state properties of $LiNbO_3$ from first-principles calculations, AIP Conf. Proc. 1675 (1) (2015), 020005.

[30] J. Yu, X. Liu, Hydrothermal synthesis and characterization of LiNbO3 crystal, Mat. Lett. 61 (2) (2007) 355−358.

[31] A.S. Andrushchak, B.G. Mytsyk, H.P. Laba, O.V. Yurkevych, I. Solskii, A.V. Kityk, B. Sahraoui, Complete sets of elastic constants and photoelastic coefficients of pure and MgO-doped lithium niobate crystals at room temperature, J. Appl. Phys. 106 (7) (2009), 073510.

[32] T. Philip, C.S. Menon, K. Indulekha, Higher order elastic constants, gruneisen parameter and lattice thermal expansion of lithium niobate, E J. Chem. 3 (3) (2016) 122−133, and references there in [15], [16], [17] and [18].

[33] W. Voigt, Lehrbuch der Kristallphysik, B. G. Teubner, Leipzig, 1928.

[34] S. Chandrasekar, S. Santhanam, A calculation of the bulk modulus of polycrystalline materials, J. Mater. Sci. 24 (12) (1989) 4265−4267.

[35] R. Hill, The elastic behaviour of a crystalline aggregate, Proc. Phys. Soc. Lond. 65 (5) (1952) 349−354.

[36] S.F. Pugh, Relations between the elastic moduli and the plastic properties of polycrystalline pure metals, Philos. Mag. 45 (367) (1954) 823−843.

[37] A. Dhar, A. Mansingh, Optical properties of reduced lithium niobate single crystals, J. Appl. Phys. 68 (11) (1990) 5804.

[38] H. Xu, D. Lee, J. He, S.B. Sinnott, V. Gopalan, V. Dierolf, S.R. Phillot, Stability of intrinsic defects and defect clusters in $LiNbO_3$ from density functional theory calculations, Phys. Rev. B 78 (17) (2008) 174103., and reference there in.

[39] C. Thierfelder, S. Sanna, A. Schindlmayr, W.G. Schmidt, Do we know the band gap of lithium niobate? Phys. Status Solidi C 7 (2) (2010) 362−365.

[40] T. Yan, Growth, Structure and Properties of High Quality LiNbO3 and LiTaO3 Crystals, Shandong University (in Chinese).

[41] V. Saleev, A. Shipilova, First-principles calculations of LiNbO3 optical properties: from far-infrared to ultraviolet, Mod. Phys. Lett. B 32 (5) (2018) 1850063.

[42] C. Kittel, Introduction to Solid State Physics, seventh ed., Wiley, 1996.

[43] S.D. Dan, W.Q. Lin, H. Chong, C. Ki, P.Y. Wu, Electronic and optical properties of lithium niobate under high pressure: a first-principles study, Chinese Phys. B 24 (7) (2015), 077104.

https://doi.org/10.1016/j.heliyon.2019.e01436